ORIGINAL PAPER

Lab Scale Fixed-Bed Reactor for Operando X-Ray Absorption Spectroscopy for Structure Activity Studies of Supported Metal Oxide Catalysts

**Santhosh Kumar Matam · O. Korsak ·
L. Bocher · D. Logvinovich · P. Hug ·
A. Weidenkaff · D. Ferri**

Abstract Lab scale fixed-bed reactor is applied for operando transmission X-ray absorption spectroscopy (XAS) for structure–activity studies of supported metal oxide catalysts under real reaction conditions. This setup includes many properties of an optimal fixed-bed reactor for operando transmission XAS studies. For instance, it is usable in a wide range of temperature (up to 1,000 °C), pressure and space velocity. Besides, this operando setup can be used for transmission XAS measurements in a wide edge energy range. The potential of this reactor for operando transmission XAS is demonstrated by, as examples, the three-way catalytic performance of $Pd/Al_2O_3/CeZrO_2$ and Rh/Al_2O_3.

Keywords Operando spectroscopy · Lab scale fixed-bed reactor · X-ray absorption spectroscopy · Structure–activity relationships

1 Introduction

Operando spectroscopy is an important field of research in heterogeneous catalysis as it provides the know-how of a catalyst and hence, it can enhance our understanding of a catalytic process. Given the importance of the operando methodology, a great deal of research has been dedicated to developing operando spectroscopy further for characterizing heterogeneous catalysts. For example, by improved reaction cell designs [1–8], coupling complementary techniques [2–15] and data analysis methods [16]. Reaction cells play an important role in operando spectroscopy as small variations in the reaction conditions (gas composition, gas flows, mass transfer effects, temperature, pressure, etc.) can dynamically transform catalyst structure which ultimately impact the catalyst performance [2]. This could provide a biased knowledge on the structure–activity relationships in catalysts. Different reaction cell designs such as capillary reactor, stainless steel block, diffuse reflectance cell (required when IR is coupled with XAS) and quartz tubes have been reported [1–10]. Undoubtedly, each of the cell designs has its own merits and demerits. These cells (except those reported very recently in [9] and [17]) were used assuming similar reaction conditions to those in a lab scale fixed-bed (or plug-flow) reactor [1–15]. In most of the cases it may be true however, some of the cell designs are often limited by gas flows, mass transfer effects, temperatures, etc.

These intrinsic limitations of reaction cells have been significantly reduced by capillary reactors for X-ray based techniques (XAS and XRD) [1]. Recently, improved but hazardous, Be tube (2–1.5 mm diameter and 10 cm length) cells were proposed over the conventional capillary reactors [18]. Our experience with capillary reactors revealed different disadvantages, for instance, pressure drop in the reactor, small gas flow rates, gradients in the large catalyst bed [19, 20] (e.g., 2 cm [1]) and a small amount of the catalyst mass probed despite large catalyst bed. Quartz reactors were also used however, with catalyst pellets instead of a catalyst bed comprising of catalyst sieve

S. K. Matam (✉) · O. Korsak · L. Bocher · D. Logvinovich ·
P. Hug · A. Weidenkaff · D. Ferri
Empa, Swiss Federal Laboratories for Materials Science
and Technology, Laboratory for Solid State Chemistry
and Catalysis, Ueberlandstrasse 129,
CH-8600 Duebendorf, Switzerland
e-mail: santhosh.matam@empa.ch

fraction, not a plug flow type reactor [7]. Very recently, a quartz reactor was reported for operando studies under conditions approaching those used for industrial operations [9, 17]. However, the reactor reported in [9] is only usable for high energy X-rays (so that these X-rays can penetrate through the thick reactor wall). For low energy X-rays, the capillary reactors have been used. Though these capillaries provide, under certain conditions, realistic reaction conditions for operando XAS studies, there is still room for improved cell designs [17].

In the present study, we report lab scale fixed-bed reactor for operando transmission XAS studies under real conditions (similar to those used for a commercial operation) using low energy X-rays. We have realized this by adapting our lab scale fixed-bed reactor comprising of quartz reactor (2 cm diameter and 45 cm length), oven, gas manifold (Bronkhorst) and mass spectrometer (MS; Balzers, Omnistar) for on line analysis of the reactor outlet at the beam line X1 of Hasylab (DESY, Hamburg, Germany).

2 Experimental

2.1 Reactor Setup

The detailed description of the setup is reported elsewhere [21]. Briefly, the reactor is typically loaded with 400 mg of catalyst (fraction of 100–150 μm) that resulted in a bed length of ca. 2 mm. The reactor is fixed in a horizontal oven placed between (I_o) and (I_1) chambers and the system is aligned such that the X-ray beam (8 × 1 mm) passes through the length of the reactor and the catalyst bed. In contrast, for a capillary reactor the X-ray beam bisects the middle of the capillary wall (or an in situ cell) and the catalyst bed [19–21]. For comparative purposes, some of the experiments were also repeated with a capillary (2.8 mm internal diameter and 7.5 cm length (Hilgenberg)) at the SuperXAS beamline, SLS (Villigen, Switzerland). The capillary is loaded with ca. 50 mg of catalyst (fraction of 100–150 μm) which resulted in a bed length of ca. 5 mm.

The potential of the operando setup was explored by studying various supported (e.g., Pd, Pt or Rh on Al_2O_3, $CeZrO_2$, $Al_2O_3/CeZrO_2$ or perovskites) catalysts on the three-way catalytic (TWC) performance, oxidation and reduction reactions. Here two examples will be discussed: (i) comparison of TWC performance of $Pd/Al_2O_3/CeZrO_2$ conducted with the present setup and with a capillary reactor and (ii) the effect of thermal aging on the redox properties of Rh supported on Al_2O_3 and its influence on the TWC properties. For the second example, the fresh and

hydrothermally aged 2 wt% Rh/Al_2O_3 are subjected to H_2-TPR and sequential CO and NO pulse experiments.

2.2 Catalysts

The catalysts 1.6 wt% $Pd/Al_2O_3/CeZrO_2$ (BET surface area: 118 m^2/g) and 2 wt% Rh/Al_2O_3 (BET: 134 m^2/g) were kindly provided by Umicore, Germany. The fresh catalysts were calcined in air at 500 °C for 4 h. A portion of the fresh catalyst Rh/Al_2O_3 was hydrothermally aged (in 10 vol% H_2O, 10 vol% O_2 in N_2) at 1,000 °C for 16 h (BET: 68 m^2/g).

2.3 Operando X-Ray Absorption Spectroscopy

The three-way catalytic performance of $Pd/Al_2O_3/CeZrO_2$ was measured with the present setup and the capillary reactor. The feed composition was 1,300 ppm CH_4, 7,000 ppm CO, 1,600 ppm NO and 5,300 ppm O_2 in He. The total flow rate was either 400 mL/min (for the present setup) or 50 mL/min (for the capillary reactor). In the former, the same flow rate was detected at the outlet of the reactor. However, the flow rate of only 30 mL/min was detected at the outlet of the capillary. This indicates that there was a pressure drop in the reactor which could not be avoided even at lower flow rates. The catalyst bed temperature in the present setup is measured through the reactor wall (by directly placing the K-type thermocouple on the reactor wall), whereas only hot air temperature estimation between the reactor and oven (air blower) is considered for a capillary reactor [1, 20, 21].

Temperature programmed reduction with H_2 (H_2-TPR) of fresh and aged Rh/Al_2O_3 were performed between room temperature and 450 °C. Prior to H_2-TPR experiments, catalysts were calcined in air at 500 °C for 30 min. After H_2-TPR, catalysts were flushed with He for 15 min at 450 °C and subsequently sequential pulses of CO/He and NO/He for 500 s each were performed. In total of eight cycles (CO + NO pulses gives rise to a cycle), first two cycles were considered to allow the system to reach steady-state.

X-ray absorption spectroscopy (XAS) data were collected in the transmission mode. X-ray absorption near edge structure (XANES) spectra were measured at the Pd K-edge (24.35 keV) to study the behaviour of Pd during the TWC over $Pd/Al_2O_3/CeZrO_2$. XANES and EXAFS (extended X-ray absorption fine structure) spectra were obtained at the Rh K-edge (23.22 keV) using Rh foil as reference. During H_2-TPR, XANES spectra were measured. Quick EXAFS spectra (125 s per spectrum) were obtained during the CO/NO pulse experiment. WINXAS v3.1 software was used for data evaluation [22].

3 Results and Discussion

3.1 The Potential of the Operando Setup is Demonstrated by Probing the TWC Performance of Pd/Al$_2$O$_3$/CeZrO$_2$ and the Redox Properties of Rh in Fresh and Aged Catalysts
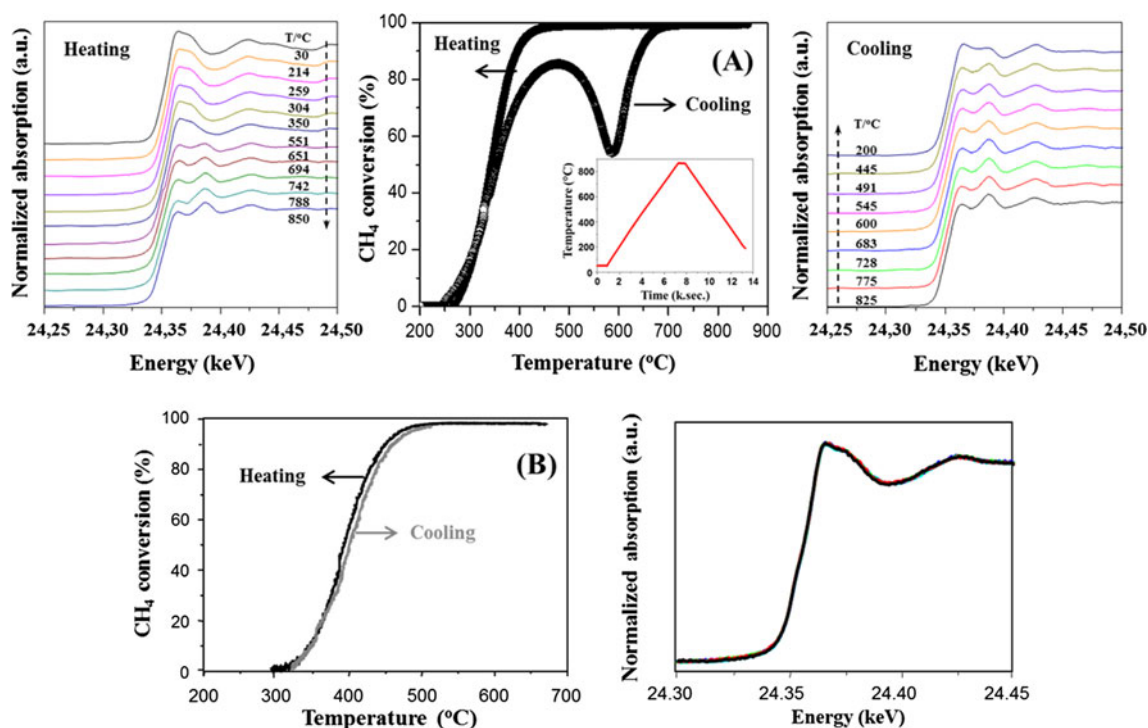
3.1.1 Three-way catalytic (TWC) performance of Pd/Al$_2$O$_3$/CeZrO$_2$

The potential of the operando setup is assessed by comparing the TWC performance of Pd/Al$_2$O$_3$/CeZrO$_2$ obtained with the lab scale fixed-bed reactor and capillary. For the sake of clarity, only the oxidation of methane profiles and the corresponding XANES spectra are shown in Fig. 1. Starting with the data obtained on the present setup, the maximum conversion of methane during heating is observed at around 445 °C and the conversion remains the same up to 860 °C (Fig. 1a). However, while cooling conversion remains the maximum up to 680 °C. Typical loss in the combustion activity is then observed between 680 and 450 °C with a maximum loss of methane conversion at around 589 °C. It is noteworthy that at 325 °C (either heating or cooling), around 30% conversion of methane is observed. The corresponding XANES measured during heating and cooling are shown in

Fig. 1a. The black spectrum (see heating) indicates the initial state of palladium in the catalyst, which is the oxidized state [21]. During heating, PdO$_x$ is reduced at around 650 °C and it remains the same up to 860 °C. While cooling, the reduced Pd only slightly reoxidizes at around 200 °C. These results reveal the occurrence of a redox cycle (reduction and re oxidation of PdO$_x$) in the catalyst under these experimental conditions. The data obtained with the capillary reactor is different as shown in Fig. 1b. No methane conversion is observed at 325 °C (either heating or cooling) and the corresponding XANES spectra show no reduction of PdO$_x$ in the catalyst even at around 680 °C (Fig. 1b). These results can be attributed to the following observations made during the experiment in the capillary reactor: (i) pressure drop in the reactor, (ii) the way the catalyst bed temperature is measured (see Fig. 2 and Sect. 2.3), (iii) space velocity or (iv) temperature (maximum T that could be attained with this capillary setup is 680 °C).

3.1.2 XANES during H$_2$-TPR

The reducibility of Rh in fresh and aged catalysts is shown in Fig. 3. The initial state of Rh after oxidative pretreatment and before H$_2$ switch (black spectra) is a completely oxidized state [19]. In the fresh catalyst, significant

Fig. 1 Three-way catalytic performance of Pd/Al$_2$O$_3$/CeZrO$_2$ obtained with the present setup (**a**) and capillary reactor (**b**). See text for experimental conditions. Temperature profile of the catalyst bed measured through the reactor wall is shown in the *inset*
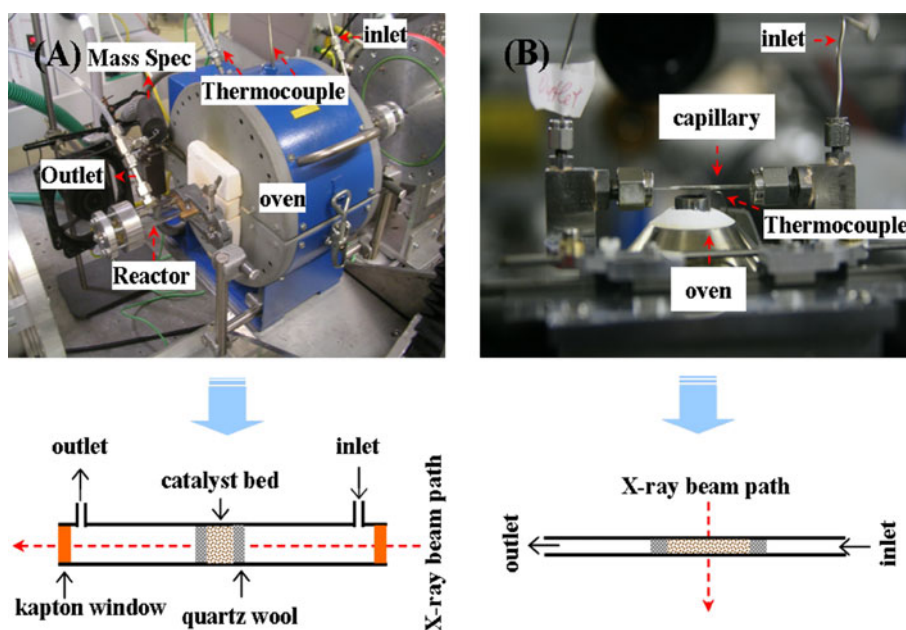
reduction of Rh is observed already at 30 °C (red spectrum) as evidenced by the decreased intensity of the white line that is accompanied by a red shift of the edge energy and appearance of a new peak at Δ keV of 0.0324. These features are characteristic for metallic Rh [19]. Complete reduction of Rh is essentially observed at around 100 °C (pink spectrum) after which the process is minimal even up to 450 °C (green spectrum). In marked contrast, most of Rh in the aged catalyst is not sensitive to reduction even up to 450 °C as evidenced by the negligible decrease in intensity of the spectra taken at 30 °C (initial spectrum, black) and 450 °C (green). This indicates that only a small fraction of Rh is reducible in the catalyst, in line with literature [23–25]. For example, it was shown that the reducibility of Rh in 0.5 wt% Rh/Al_2O_3 decreases with increasing aging temperature by H_2-TPR. And, only 14% Rh is reducible in the catalyst that was aged at 702 °C for 1 h [25]. However, such a behaviour of Rh is not yet completely understood and different mechanisms were proposed [23, 26]. Our recent findings by UltraSTEM suggest that the diffusion of Rh into the alumina lattice is responsible for highly reduction resistant Rh oxide formation [27].

3.1.3 Quick EXAFS during Sequential CO and NO Pulses over Reduced Catalysts

The reaction between CO and NO is one of the most important steps in three-way catalytic processes for the oxidation and reduction of CO and NO, respectively, over Rh [28–31]. Thus, the behaviour of Rh during the transient reaction between CO and NO over the reduced fresh Rh/Al_2O_3 catalyst at 450 °C is studied by quick EXAFS (Fig. 4). Every CO or NO gas pulse was sequentially

switched on for 500 s for a total of eight cycles, starting with CO pulse.

During each pulse, four quick EXAFS were measured. For the sake of clarity, only the last spectrum (i.e., the fourth spectrum) from each switch and two spectra from a total of eight spectra for a complete CO/NO cycle are shown in Fig. 4. Only three complete switches from a total of eight are shown for MS data (Fig. 4). A set of 16 quick EXAFS during two complete CO and NO cycles can be found in ESI (Fig. S1).

After a reductive pretreatment, Rh is in a completely reduced state. A subsequent CO switch does not change the state of Rh in the catalyst as evident from the spectrum (black) in Fig. 4 that is similar to the spectrum (green) taken at 450 °C during H_2-TPR (Fig. 3). The reduced Rh is partly reoxidized upon subsequent NO switch indicating that Rh is redox active in the fresh catalyst. A sharp evolution of products CO_2 and N_2 is also evident from the corresponding MS data on either a CO or NO switch. Based on these observations it can be suggested that the redox cycle involving surface reaction between CO and NO is occurring on Rh as shown in Eq. 1.
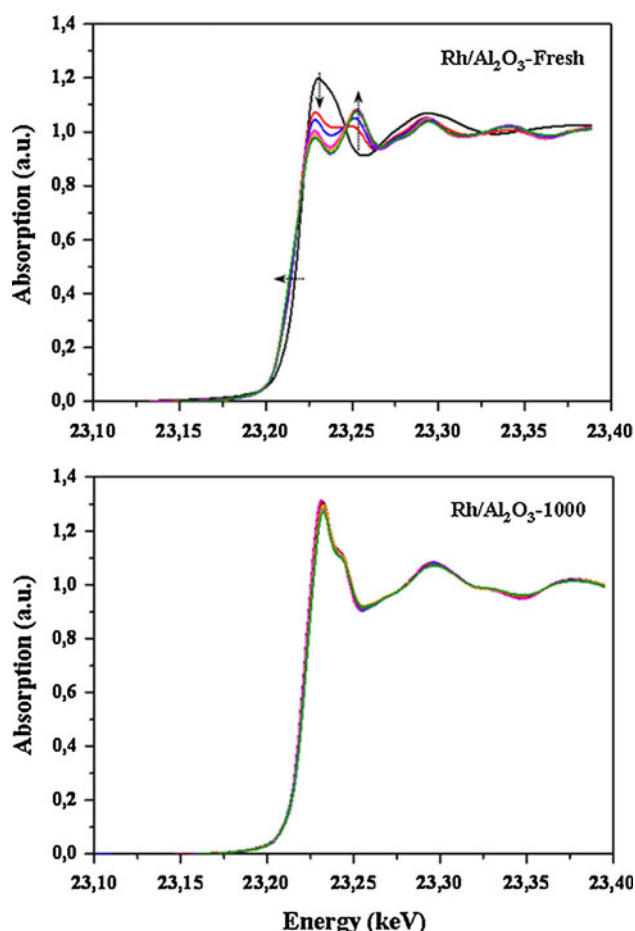
$$CO \ + \ NO \ \rightarrow \ CO_2 + \tfrac{1}{2}N_2 \qquad (1)$$
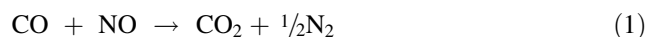
The mass fraction ($m/z = 44$) of CO_2 overlaps with that of N_2O. Thus the formation of the latter cannot be ruled out according to the Eq. 2.

$$CO \ + \ 2NO \ \rightarrow \ CO_2 + \ N_2O \qquad (2)$$
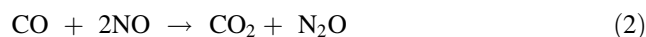
Evidence on the occurrence of these two reactions is reported elsewhere [16], where we have studied CO/NO cycles on on Rh/A_2O_3 by energy dispersive EXAFS/ DRIFTS/MS. It was observed that upon a CO switch the
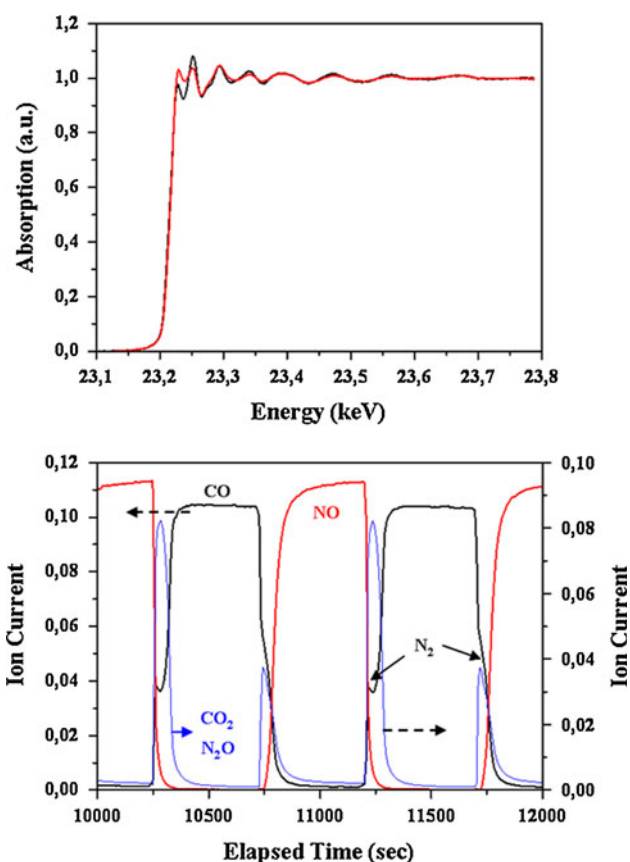
Fig. 3 XANE spectra of the catalysts during heating from 30 to 450 °C (5 °C/min) in a flow of 5 vol% H_2/He. Initial spectra at 30 °C (*black*) and spectra at 450 °C (*green*)

Fig. 4 Sequential pulses between 1 vol% CO/He and 1 vol% NO/He over pre-reduced fresh Rh/Al_2O_3 catalyst at 450 °C. The quick EXAFS during pulses (*above*) and relative concentration of reactants (CO and NO) and products (CO_2, N_2O and N_2) at the outlet of the reactor is analyzed on-line by MS (*below*)

catalyst surface is populated by differently adsorbed CO species. A subsequent NO switch produces CO_2 via Rh-NCO species (Eq. 1) and N_2O via formation of Rh-NO^-(Eq. 2).

Interestingly, the relative intensity of MS signal of $m/z = 44$ associated to CO_2 and N_2O is different between the CO → NO and the NO → CO switches (Fig. 4). The signal intensity is always higher for the latter switch than for the former. It may suggest that during NO → CO switch the formation of products is significant, especially N_2O, than that during CO → NO switch. This could be due to more available Rh sites for NO to form species like Rh-NO^- and to the partially oxidized state of Rh, which are responsible for N_2O formation [16].

In contrast to the fresh catalyst, as evident from Fig. 3, most of Rh is not redox active in the hydrothermally aged catalyst during CO/NO cycles (Fig. S1 in ESI). This could explain the poor TWC performance of the catalyst [24, 25].

3.2 Advantages and Limitations of the Operando Setup

3.2.1 Advantages

The photographs and schematic diagrams of the operando setup and capillary reactors are depicted in Fig. 2. The main advantages of the setup are as follows:

(i) The typical catalyst bed length is around 2 mm in the reactor which is much smaller than that often used in a conventional operando reaction cell for example 1–2 cm [1, 4]. This implies that the concentration gradients within the solid phase and gas–solid phases can be greatly reduced.

(ii) The X-ray beam probes the whole catalyst bed length (from front to rear), averaging out, if any, gradients in the catalyst bed of 2 mm. This in turn prevents the loss of spatiotemporal information [9].

(iii) The volume of the catalyst probed in the reactor is more than one order of magnitude larger than that in

conventional operando reaction cells. This allows to obtain high-quality spectra.

(iv) The setup allows for studying catalysis under a large window of space velocities which is extremely limited with operando reaction cells. This implies that a reaction can be performed under a kinetically controlled regime.

The above advantages demonstrate that accurate and reliable data on the catalyst structure activity relationships can be obtained with this setup. Furthermore, the reactor setup can directly be coupled with operando UV–Vis and Raman spectroscopic techniques.

3.2.2 Limitations

The setup is limited by the large reactor volume that has the following main implications:

(i) The catalyst bed length is much smaller (between 2 and 4 mm, which is suitable for operando studies) than that of in an optimal reactor (in this case it should have been 20 cm). This is a compromise between the bed length and spatiotemporal information along the bed, the smaller the bed the better the received spatiotemporal information.

(ii) Though the setup can be used in a wide space velocity, it may not be suitable for very low space velocity regimes.

(iii) Unlike capillary reactors, this setup cannot be coupled with XRD.

4 Conclusions

A lab scale fixed-bed reactor is presented that allows to conduct operando transmission X-ray absorption spectroscopy studies under an optimal reaction conditions of a fixed-bed reactor and to obtain high quality data. With this setup the loss of spatiotemporal information can be greatly avoided. The obtained results demonstrate the participation of Pd and Rh redox cycle in TWC process which in turn proved the credibility of the setup.

References

1. Clausen BS, Fabius GSB, Villadsen J, Feidenhans'l R, Topsoe H (1991) J Catal 132:524
2. Topsoe H (2003) J Catal 216:155
3. Sankar G, Thomas JM (1999) Top Catal 8:1
4. Odzak JF, Argo AM, Lai FS, Gates BC, Pandya K, Feraria L (2001) Rev Sci Instrum 72:3943
5. Weckhuysen BM (2002) Chem Commun 58:97
6. Grunwaldt J-D, Clausen BS (2002) Top Catal 18:37
7. Bare SR, Mickelson GE, Modica FS, Ringwelski AZ, Yang N (2006) Rev Sci Instrum 77:023105
8. Mesu JG, van der Eerden AMJ, de Groot FMF, Weckhuysen BM (2005) J Phys Chem B 109:4042
9. O'Brien MG, Beale AM, Jacques SDM, Michiel MD, Weckhuysen BM (2010) Appl Catal A 391:468
10. Tromp M, Sietsma JRA, van Bokhoven JA, van Strijdonck GPF, van Haaren RJ, van der Eerden AMJ, van Leeuwen PWNM, Koningsberger DC (2003) Chem Commun 1:128
11. Nijhuis TA, Tinnemans SJ, Visser T, Weckhuysen BM (2003) Phys Chem Chem Phys 5:4361
12. Hunger M, Wang W (2004) Chem Commun 5:584
13. Thibault-Starzyk F, Gil B, Aiello S, Chevreau T, Gilson JP (2004) Micropor Mesopor Mater 67:107
14. Grunwaldt J-D, Caravati M, Hannemann S, Baiker A (2004) Phys Chem Chem Phys 6:3037
15. Brueckner A (2005) Chem Commun 13:1761
16. Ferri D, Santhosh Kumar M, Wirz R, Eyssler A, Korsak O, Hug P, Weidenkaff A, Newton MA (2010) Phys Chem Chem Phys 12:5634
17. Bare SR, Kelly SD, Ravel B, Greenlay N, King L, Mickelson GE (2010) Phys Chem Chem Phys 12:7702
18. Bare SR, Yang N, Kelly SD, Mickelson GE, Modica FS (2007) Catal Today 126:18
19. Grunwaldt J-D, Hannemann S, Schroer CG, Baiker A (2006) J Phys Chem B 110:8674
20. Kimmerle B, Grunwaldt J-D, Baiker A, Glatzel P, Boye P, Stephan S, Schroer CG (2009) J Phys Chem C 113:3037
21. Santhosh Kumar M, Aguirre MH, Weidenkaff A, Ferri D (2010) J Phys Chem C 114:9439
22. Ressler T (1998) J Synchrotron Radiat 5:118
23. Dohmae K, Nagai Y, Tanabe T, Suzuki A, Inada Y, Nomura M (2008) Surf Interface Anal 40:1751
24. Yao HC, Stepien HK, Gandhi HS (1980) J Catal 61:547
25. Wong C, McCabe RW (1989) J Catal 119:47
26. Dohmae K, Nonaka T, Seno Y (2005) Surf Interface Anal 37:115
27. Bocher L, Aguirre MH, March K, Kumar MS, Ferri D, Colliex C, Stéphan O (2010) 7th International Microscopy Congress (IMC17). Rio de Janeiro, Brazil
28. Peden CHF, Goodman DW, Blair DS, Berlowitz PJ, Fisher GB, Oh SH (1988) J Phys Chem 92:1563
29. Permana H, Ng KYS, Peden CHF, Schmieg SJ, Belton DN (1995) J Phys Chem 99:16344
30. Dent AJ, Evans J, Fiddy SG, Jyoti B, Newton MA, Tromp M (2007) Angew Chem Int Ed 46:5356
31. Chafik T, Kondarides DI, Verykios XE (2000) J Catal 190:446